Electric Field Cancellation on Quartz by Rb Adsorbate-Induced Negative Electron Affinity

J. A. Sedlacek,[1] E. Kim,[2] S. T. Rittenhouse,[3,4] P. F. Weck,[5] H. R. Sadeghpour,[6] and J. P. Shaffer[1,*]
[1]*Homer L. Dodge Department of Physics and Astronomy, The University of Oklahoma, Norman, Oklahoma 73019, USA*
[2]*Department of Physics and Astronomy, University of Nevada Las Vegas, Las Vegas, Nevada 89154, USA*
[3]*Department of Physics and Astronomy, Western Washington University, Bellingham, Washington 98225, USA*
[4]*Department of Physics, The United States Naval Academy, Annapolis, Maryland 21402, USA*
[5]*Sandia National Laboratories, Albuquerque, New Mexico 87185, USA*
[6]*ITAMP, Harvard-Smithsonian Center for Astrophysics, Cambridge, Massachusetts 02138, USA*
(Received 24 November 2015; published 30 March 2016)

We investigate the (0001) surface of single crystal quartz with a submonolayer of Rb adsorbates. Using Rydberg atom electromagnetically induced transparency, we investigate the electric fields resulting from Rb adsorbed on the quartz surface, and measure the activation energy of the Rb adsorbates. We show that the adsorbed Rb induces negative electron affinity (NEA) on the quartz surface. The NEA surface allows low energy electrons to bind to the surface and cancel the electric field from the Rb adsorbates. Our results will be important for integrating Rydberg atoms into hybrid quantum systems, as fundamental probes of atom-surface interactions, and for studies of 2D electron gases bound to surfaces.

DOI: 10.1103/PhysRevLett.116.133201

Because of recent technological advances in fabrication and trapping, hybrid quantum systems (HQS) consisting of atoms and surfaces, as well as electrons and surfaces, are fast emerging as ideal platforms for a diverse range of studies in quantum control, quantum simulation, and computing, strongly correlated systems, and microscopic probes of surfaces [1–5]. Miniaturization of chip surfaces is necessary to achieve large platform scalability, but decoherence and noise emerge as serious challenges as feature sizes shrink [6–8]. Mitigating noise is a fundamental step in realizing the full potential of HQS.

Combining ultracold Rydberg atoms with surfaces for HQS is attractive because Rydberg atoms can have significant transition dipole moments and strong interactions. There have been a host of theoretical proposals recently for utilizing Rydberg atoms near surfaces [2,9–12]. Experimental progress has been hampered by uncertainties in characterizing the interactions of the atoms with the surfaces, although some recent work in this regards is noteworthy [13–15].

To take full advantage of Rydberg atom HQS, a more complete understanding of surfaces is needed. One problem is that Rydberg atoms incident upon metal surfaces can be ionized [16,17]. A second major hurdle is the background electric fields (E fields) caused by adsorbates [18–23]. Rydberg states are sensitive to adsorbate E fields because they are highly polarizable [24]. Adsorbate E fields have caused problems for other experiments as well, including Casimir-Polder measurements [25] and surface ion traps [26]. A possible solution is to minimize the E fields by canceling them out.

A convenient surface for applications in HQS is quartz because of its extensive use in the semiconductor and optics industries. Despite numerous theoretical and experimental studies of bulk SiO_2 [27–29], the surface properties are not well understood. The (0001) surface has been the subject of recent theoretical interest, partially due to its stability and low surface energy [30–34].

In this work, we show that a quartz (0001) surface with Rb adsorbates, contrary to the prevailing assumption, can have very small E fields near the surface, Fig. 1(c). We demonstrate, by appealing to theoretical arguments and *ab initio* calculations, that the reduction in the E field is caused by a transformation of the quartz into a negative electron affinity (NEA) surface via adsorption of Rb atoms on the surface. A NEA surface can bind electrons, similar to the image potential states on liquid helium (LHe) [35–37]. While the surface repulsion for electrons on LHe is provided by Pauli blocking, the repulsion on quartz occurs because the surface vacuum level dips below the conduction band minimum. We find that the binding of electrons to the surface substantially reduces the E field above the surface.

In experiments on atom-adsorbate interactions, using different surfaces, adsorbate E fields with magnitudes ranging from $\sim$0.1–10 $\mathrm{V\,cm^{-1}}$ have been measured at distances of $\sim$10–100 μm [13,19,20,22,25]. We measure radically different E fields dependent upon the number of slow electrons produced by Rydberg atoms near the surface. We demonstrate that E fields as small as 30 $\mathrm{mV\,cm^{-1}}$ can be obtained 20 μm from the surface.

A microscopic picture of E field noise is obtained by considering thermal fluctuations of adsorbate dipole moments [38]. An adsorbed atom develops a dipole moment as a result of the polarization of the adatom in interaction with the surface. As the density of adsorbates

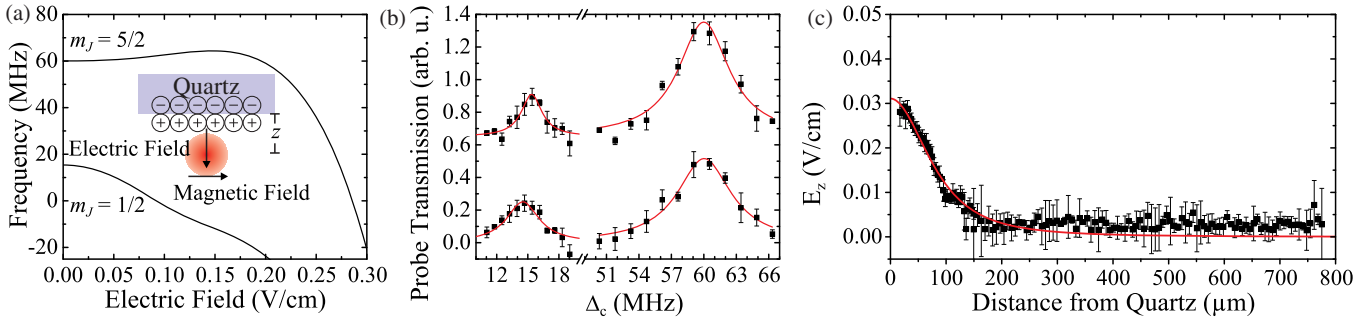

FIG. 1. (a) Stark shift for $81D_{5/2}$, $m_J = 5/2$ and $1/2$ states in a 14.3 G magnetic field oriented perpendicular to the E field. The inset shows the orientation of the electric and magnetic fields with respect to the quartz surface. (b) EIT spectra taken at two different positions $z = 150$ μm (upper) and $z = 50$ μm (lower) for $81D_{5/2}$ $m_J = 1/2$ (left) and $m_J = 5/2$ (right). The black points are pixel values of three averaged images, and the error bars are the standard deviation of the pixel values. The red lines are Lorentzian fits to the data. At $z = 50$ μm the $m_J = 1/2$ state is broadened and shifted corresponding to an E field of 0.02 V cm^{-1}. (c) In the limit of large numbers of Rydberg atoms [Rb($81D$)], population the E field is measured at distances of ~20–800 μm from the quartz surface at $T_{\text{sub}} = 79\,^{\circ}$C. Black points are taken from different pixels on a CCD camera. The error bars are the standard deviation of the measurement. The red line is a fit to Eq. (1), showing the inhomogeneity of the E field. Our calculations indicate that the E field at $z < 200$ μm is caused by the large spacing between the electrons.

increases, the E field from neighboring dipoles reduces the dipole moment of each adatom (see the Supplemental Material [39]). We estimate the dipole moment for a Rb adsorbate in the limit of small coverage to be $d_0 = 12$ D (see the Supplemental Material [39]).

Adsorption of a large number of Rb atoms on the quartz surface produces macroscopic E fields. At distances far from the surface, the E field can be modeled as two square sheets of charge, with edge length L, separated by a small distance [21,22]. Near the center of the sheets, the E field is largely perpendicular to the surface

$$E_z(z) = \frac{2\sqrt{2}\sigma d(\sigma) L^2}{\pi\epsilon_0\sqrt{L^2+2z^2}(L^2+4z^2)}, \tag{1}$$

where ϵ_0 is the permittivity of free space, σ is the adsorbate density, and $d(\sigma)$ is the coverage dependent dipole moment. The temperature dependence of σ is [54]

$$\frac{\sigma/\sigma_0}{1-\sigma/\sigma_0} = Ce^{(E_a/kT_{\text{sub}})}, \tag{2}$$

where σ_0 is the density of adsorbate sites, E_a is the desorption activation energy, k is the Boltzmann constant, and T_{sub} is the substrate temperature. Equations (1) and (2) relate E_z to σ at T_{sub}.

The E fields are determined experimentally by measuring the frequency shift of a Rydberg state, and comparing it to a Stark shift calculation. Stark shifts of two magnetic states for $81D_{5/2}(m_J = 5/2$ and $m_J = 1/2)$ are shown in Fig. 1(a). An example of the experimental traces at different z is shown in Fig. 1(b). These types of traces were used to obtain the E fields. The Rydberg state energy is determined using Rb Rydberg atom electromagnetically induced transparency (EIT) [55]. The energy level scheme is shown in Fig. 2(a). The Rydberg EIT is detected by the absorption of the probe laser by the atomic cloud on a CCD camera [20–22], Fig. 2(b). The E field and its spatial dependence are obtained by analyzing the absorption images as a function of coupling laser detuning with a spatial resolution of 5.5 μm.

For the experiments, a mirror magneto-optical trap (MOT) is used to load a Rb magnetic trap ~2 mm from the quartz surface, Fig. 2(b). After loading the magnetic trap, bias magnetic fields are used to move the atoms close to the surface. The atoms are released from the magnetic

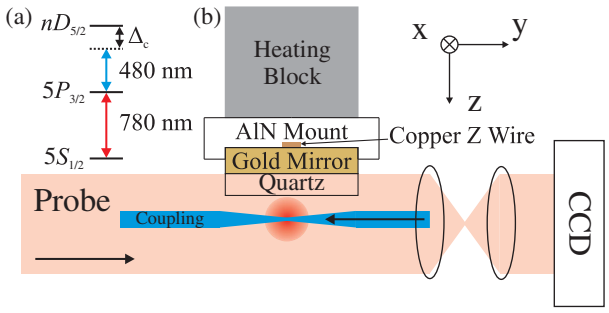

FIG. 2. (a) Level scheme for Rydberg EIT used in our experiments. Δ_C is the coupling laser detuning. (b) A schematic of the experimental setup. Rb atoms are trapped in a mirror MOT, transferred into a magnetic trap, and transported to the surface. The probe and coupling beams for Rydberg EIT are overlapped and counterpropagate. The Rydberg EIT signal is observed by analyzing the absorption of the probe beam on a CCD camera. Heaters are placed outside of the vacuum to control the quartz temperature. The gold mirror is used to form the MOT. The heating block controls the temperature of the substrate. The Z wire generates the magnetic trap. The aluminum nitride (AlN) mount insulates the Z wire from the heating block.

trap and imaged. The atomic cloud is a cigar shaped Gaussian cloud with $1/e^2$ radii of $0.5 \times 0.5 \times 1$ mm.

At low Rydberg atom numbers, the E field is homogeneous over the magnetic trap because the EIT signal is not detectably broadened across the extent of the atom sample, ~2 mm. The variation of the E field over $z =$ 200–1000 μm is < 0.1 V cm^{-1}, Fig. 1(c). The sensitivity is limited by the polarizability of the Rydberg state. L is estimated to be 10 mm and is similar in size to other observations [21].

The main source of the Rb adsorbate E field is the MOT atoms. Disabling the magnetic trap for ~10 min did not change the E field. Disabling the MOT for the same period changes the E field. In the presence of the MOT, the adsorbate coverage can be controlled by changing the surface temperature.

The adsorbate E field points away from the surface as confirmed by an external compensating E field. The adsorbate E field is estimated to be normal to the surface, within 15°, based on the differential shifts of different m_J states. This further justifies the model in Eq. (1).

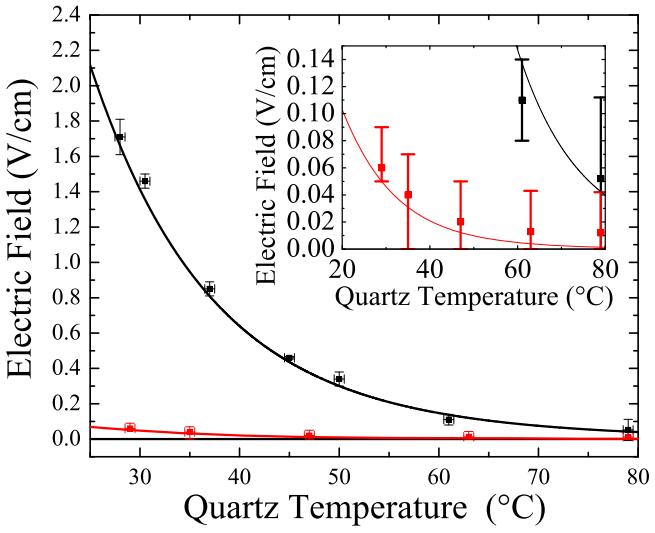

FIG. 3. The measured E fields due to Rb adsorbates on the (0001) surface of quartz as a function temperature T_{sub} at a distance of 500 μm from the surface. The E fields are calculated by analyzing the frequency shifts of the EIT spectra. The black points are in the limit of low Rydberg atom production. The black line is a fit to the Langmuir isobar of Eq. (2), and yields a desorption activation energy of $E_a = 0.66 \pm 0.02$ eV. The red data points were taken with high Rydberg atom production. The red line is explained in the text. The horizontal error bars are due to the uncertainty in the temperature T_{sub}. The vertical errors bars are the standard deviation of the experimental data. In the case of high- (low-) Rydberg atom production, the Rabi frequencies of the probe and coupling lasers are $\Omega_p = 2\pi \times 3.5\,(0.5)$ MHz and $\Omega_c = 2\pi \times 4\,(4)$ MHz. Approximately 200 (10) electrons are produced during each experimental sequence, with a 10 (0.5) Hz average rate. The horizontal error bars are due to the uncertainty in T_{sub} and are ±0.5 °C.

We measured the E field as a function of T_{sub}. The results are shown in Fig. 3 at $z = 500$ μm. At 28 °C, the E field is 1.7 ± 0.1 V cm^{-1}. Using Eq. (1), for a slab of length $L = 10$ mm and $d_0 \sim 12$ D, we estimate $\sigma = 4 \times 10^5$ atoms μm^{-2}, yielding an average Rb spacing of ~1.5 nm, and an adatom coverage of 11%. Fitting all values of σ to Eq. (2) with a coverage dependent dipole moment yields $E_a = 0.66 \pm 0.02$ eV. E_a is similar to the activation energy measured for alkali atoms on similar surfaces [56–59].

Increasing the Rydberg atom number in either trap dramatically reduces the E field, by increasing the flux of slow blackbody ionized electrons that can bind to the surface. The Rydberg atom number can be made larger by increasing the probe laser Rabi frequency. The temperature dependence of the reduced E field is shown in Fig. 3. For typical data in Fig. 3, 300 atoms are ionized per experimental sequence. Rb(nS) and Rb(nD) states were investigated for $40 \leq n \leq 100$, yielding similar results.

The Rydberg atoms are predominately ionized due to blackbody radiation; direct blackbody ionization accounts for 99% of all electrons [60] at high n. For Rb($81D_{5/2}$), the electrons have an average kinetic energy of 10 meV. For $n \sim 40$–100, the electrons average kinetic energy is 8–15 meV [61].

If blackbody ionized electrons can bind to the surface, they can neutralize the E field produced by the Rb adatoms. Electrons can bind to a conducting or dielectric surface through their image potential [62]. These states are usually ultrashort lived, and rapidly collapse into the bulk. In LHe, however, the Pauli repulsion provides the necessary barrier of ~1 eV to prevent decay, leading to the formation of stable bound states on the surface. In LHe, the electrons can remain in these states for tens of hours at cryogenic temperatures [37]. For adsorption on ordinary surfaces, if the vacuum energy dips below the bottom of the conduction band, a NEA surface is produced, repelling electrons from the surface.

Amorphous quartz has a positive electron affinity of 0.9 eV [63]. However, the adsorption of atoms can change the surface properties. The dipole layer created by the adsorbates changes the electric potential at the vacuum-surface interface. By calculating the electrostatic change in energy of an electron across the surface dipole layer, an estimate of the change in electron affinity $\Delta\chi$ can be made [64] (see the Supplemental Material [39]). Using $d_0 =$ 12 D and $\sigma = 4.2 \times 10^5$ atoms μm^{-2} at $T_{\text{sub}} = 28$ °C, the change in surface electron affinity is $\Delta\chi = -1.9$ eV. This approximation suggests that Rb at our densities can shift the vacuum level ~1 eV below the conduction band, inducing a NEA surface on quartz. The model shows a NEA up to $T_{\text{sub}} \sim 40$ °C.

To investigate the adatom-surface on a microscopic level, we performed total-energy calculations for the quartz (0001) surface with various Rb coverages using

spin-polarized density functional theory (DFT) [65] (see the Supplemental Material [39]). On the surface of quartz, the Rb atom is bound to two oxygen atoms. The lowest bound state for one monolayer (ML) has an energy of $E_b = 0.35$ eV. For the lower experimentally investigated coverages, our DFT calculations show an increase of E_b by ~1.4. The calculated E_b is comparable in magnitude with the measured E_a, and is consistent with the expectation $E_b \leq E_a$ [66].

We calculated the electronic density of states for bulk α-quartz and the shift of the vacuum energy with varying amounts of Rb coverage using DFT, Fig. 4. The Fermi level E_F is set equal to zero, and lies in the middle of the band gap, between the top of the valance band $E_{v,\mathrm{bulk}} = -3.05$ eV, and the bottom of the conduction band $E_{c,\mathrm{bulk}} = 3.05$ eV. As shown in Fig. 4, the vacuum level for the clean surface, $\bar{V}_{\mathrm{clean}}(\infty)$, has a positive electron affinity, consistent with experiment [63]. However, adsorbing Rb on the surface shifts the vacuum level downward. A NEA is induced around 0.5 ML. The DFT and the straightforward electrostatic calculations both show that the vacuum level shifts by several electron volts with only a modest amount of Rb coverage. The remaining discrepancy may be resolved with further improvements in DFT [67,68]. More knowledge of the experimental surface including the Rb adsorbate structure will also help to guide the calculations.

We model the electrons as a uniformly charged square sheet of length L, which overlays the adsorbate layers with $L = 10$ mm at $z = 0$. The resulting E field is a sum of the E fields from the adsorbates and electrons, $E_{\mathrm{tot}} = E_{\mathrm{ads}} + E_{\mathrm{ele}}$. After requiring $E_{\mathrm{tot}} = 0$ at $z = 0$, $E_{\mathrm{tot}}(z = 500\ \mu\mathrm{m})$ is plotted in Fig. 3. The near exact fit to the data is an indication that the reduction in the E field is due to the formation of a NEA surface for Rb-SiO_2.

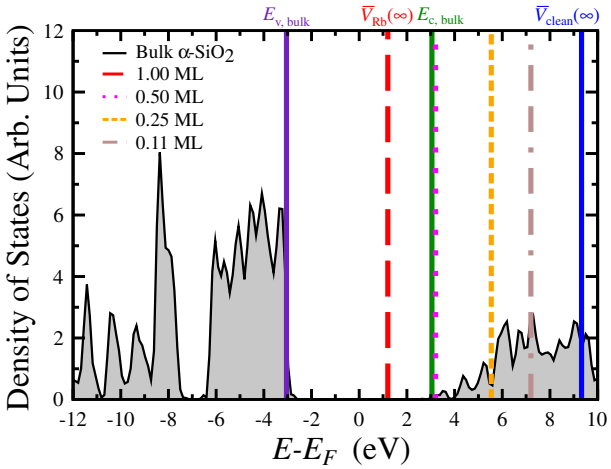

FIG. 4. Density of states of bulk α-quartz. The Fermi level E_F is at $E = 0$. The valence band maximum $E_{v,\mathrm{bulk}}$ and conduction band minimum $E_{c,\mathrm{bulk}}$ of bulk α-quartz, and the vacuum levels of the $SiO_2(0001)$ surface without and with Rb adsorbates, respectively, $\bar{V}_{\mathrm{clean}}(\infty)$ and $\bar{V}_{\mathrm{Rb}}(\infty)$, are labeled. $\bar{V}_{\mathrm{Rb}}(\infty)$ is shown as a function of coverage in fractions of a monolayer (ML). Increasing the amount of Rb coverage shifts the vacuum level down in energy. With one ML of Rb on the surface (red line), the vacuum energy dips below the bottom of the conduction band (green line), indicating the formation of a NEA surface.

For high temperatures and a high Rydberg population the E field is low. The measured E field as a function of z at $T_{\mathrm{sub}} = 79\,^{\circ}\mathrm{C}$ is shown in Fig. 1(c). For $z > 200\ \mu$m the E field is negligible within error. At $z < 200\ \mu$m the E field increases to ~30 mV cm^{-1}. Under these conditions, we estimate a surface electron density of ~10 electron mm^{-2}. For $z < 200\ \mu$m, approximating the electrons as a uniform sheet of charge breaks down since the electron spacing becomes larger than z. The spectral width of the EIT resonance for $81D_{5/2}(m_J = 1/2)$ increases from 2 MHz far from the surface to ~4 MHz at $z \leq 50\ \mu$m, Fig. 1(b). We attribute this broadening to the inhomogeneity of E_{tot} near the surface. The data in Fig. 1(c) are fit to Eq. (1), and show that the residual E field can be modeled as a dipole patch, with $L \sim 200\ \mu$m, approximately equal to the estimated electron spacing of ~300 μm.

We can remove electrons from the surface using 400 nm light generated by a light emitting diode array. With the surface saturated with electrons $[E_{\mathrm{tot}}(z = 0) = 0]$, the light emitting diodes are pulsed on for a variable time while atoms are loaded into the MOT. The light intensity is small to avoid the light induced desorption of Rb. The MOT fluorescence is monitored to verify this condition. The photodesorption rate constant has an Arrhenius behavior, with an activation energy of 0.7 ± 0.07 eV (see the Supplemental Material [39]). The activation energy is similar to E_a, suggesting the electron detachment mechanism is dependent on Rb coverage. The Rb coverage affects the energy levels most strongly. It is unknown if the electrons are detached from or tunnel into the surface. The electron photodetachment is the subject of future investigation.

Over the temperature range investigated, $28 < T_{\mathrm{sub}} < 80\,^{\circ}\mathrm{C}$, the Rb-quartz system can bind electrons for several hours, when the MOT is on and the EIT lasers are off. The small E fields have been repeatably measured many times for over a year, yielding the same results within experimental error. The thermal wavelength of an electron at 28 °C is 4.3 nm, indicating that the electron is not localized on one Rb adsorbate. We believe that the single crystal nature of the quartz and small surface roughness < 5 Å play an important role in the uniformity of the Rb adsorbates and electron binding. We have done some simulations investigating whether the dipole potential from a patch of adsorbates or the image potential is responsible for binding the electrons to the surface. Our results show that binding is due to the image potential of the electron. The dipole potential slightly shifts the image potential.

In summary, we have measured the activation energy of Rb on the quartz (0001) surface and have shown the onset

of a NEA surface capable of binding electrons upon Rb adsorption. Reducing the E fields on a quartz surface by making quartz a NEA surface by Rb adsorption is a promising pathway for coupling Rydberg atoms to surfaces. Further work can be directed towards measurements of other surface orientations and dielectrics, as well as investigating the behavior at cryogenic temperatures. The properties of the electrons, including the binding energy, mobility, and effective mass, are the subject of future work.

Sandia National Laboratories is a multiprogram laboratory managed and operated by Sandia Corporation, a wholly owned subsidiary of Lockheed Martin Corporation, for the U.S. Department of Energy's National Nuclear Security Administration under Contract No. DE-AC04-94AL85000. This work was supported by the DARPA Quasar program by a grant through ARO (Grant No. 60181-PH-DRP), AFOSR (Grant No. FA9550-12-1-0282), NSF (Grants No. PHY-1104424) and No. NSF PHY-1516421) and an NSF grant through ITAMP at the Harvard-Smithsonian Center for Astrophysics. The authors thank Tilman Pfau for useful discussions.

*shaffer@nhn.ou.edu

[1] *Atom Chips*, 1st ed., edited by J. Reichel and V. Vuletic (Wiley-VCH, New York, 2011).
[2] G. Kurizki, P. Bertet, Y. Kubo, K. Mølmer, D. Petrosyan, P. Rabl, and J. Schmiedmayer, Quantum technologies with hybrid systems, Proc. Natl. Acad. Sci. USA **112**, 3866 (2015).
[3] Z.-L. Xiang, S. Ashhab, J. Q. You, and F. Nori, Hybrid quantum circuits: Superconducting circuits interacting with other quantum systems, Rev. Mod. Phys. **85**, 623 (2013).
[4] C. Dong, Y. Wang, and H. Wang, Optomechanical interfaces for hybrid quantum networks, Natl. Sci. Rev. **2**, 510 (2015).
[5] C. Sias and M. Köhl, Hybrid quantum systems of ions and atoms, arXiv:1401.3188.
[6] R. O. Behunin, Y. Zeng, D. A. R. Dalvit, and S. Reynaud, Electrostatic patch effects in Casimir-force experiments performed in the sphere-plane geometry, Phys. Rev. A **86**, 052509 (2012).
[7] M. Brownnutt, M. Kumph, P. Rabl, and R. Blatt, Ion-trap measurements of electric-field noise near surfaces, Rev. Mod. Phys. **87**, 1419 (2015).
[8] J. D. Carter and J. D. D. Martin, Coherent manipulation of cold Rydberg atoms near the surface of an atom chip, Phys. Rev. A **88**, 043429 (2013).
[9] D. Petrosyan, G. Bensky, G. Kurizki, I. Mazets, J. Majer, and J. Schmiedmayer, Reversible state transfer between superconducting qubits and atomic ensembles, Phys. Rev. A **79**, 040304 (2009).
[10] H. Kübler, D. Booth, J. Sedlacek, P. Zabawa, and J. P. Shaffer, Exploiting the coupling between a Rydberg atom and a surface phonon polariton for single-photon subtraction, Phys. Rev. A **88**, 043810 (2013).
[11] J. D Pritchard, J. A. Isaacs, M. A. Beck, R. McDermott, and M. Saffman, Hybrid atom-photon quantum gate in a superconducting microwave resonator, Phys. Rev. A **89**, 010301 (2014).
[12] E. A. Hinds, K. S. Lai, and M. Schnell, Atoms in micron-sized metallic and dielectric waveguides, Phil. Trans. R. Soc. A **355**, 2353 (1997).
[13] C. Hermann-Avigliano, R. C. Teixeira, T. L. Nguyen, T. Cantat-Moltrecht, G. Nogues, I. Dotsenko, S. Gleyzes, J. M. Raimond, S. Haroche, and M. Brune, Long coherence times for Rydberg qubits on a superconducting atom chip, Phys. Rev. A **90**, 040502 (2014).
[14] T. Thiele, S. Filipp, J. A. Agner, H. Schmutz, J. Deiglmayr, M. Stammeier, P. Allmendinger, F. Merkt, and A. Wallraff, Manipulating Rydberg atoms close to surfaces at cryogenic temperatures, Phys. Rev. A **90**, 013414 (2014).
[15] R. C. Teixeira, C. Hermann-Avigliano, T. L. Nguyen, T. Cantat-Moltrecht, J. M. Raimond, S. Haroche, S. Gleyzes, and M. Brune, Microwaves Probe Dipole Blockade and van der Waals Forces in a Cold Rydberg Gas, Phys. Rev. Lett. **115**, 013001 (2015).
[16] S. B. Hill, C. B. Haich, Z. Zhou, P. Nordlander, and F. B. Dunning, Ionization of Xenon Rydberg Atoms at a Metal Surface, Phys. Rev. Lett. **85**, 5444 (2000).
[17] E. So, M. Dethlefsen, M. Ford, and T. P. Softley, Charge Transfer of Rydberg H Atoms at a Metal Surface, Phys. Rev. Lett. **107**, 093201 (2011).
[18] H. Kübler, J. P. Shaffer, T. Baluktsian, R. Löw, and T. Pfau, Coherent excitation of Rydberg atoms in micrometre-sized atomic vapour cells, Nat. Photonics **4**, 112 (2010).
[19] J. D. Carter, O. Cherry, and J. D. D. Martin, Electric-field sensing near the surface microstructure of an atom chip using cold Rydberg atoms, Phys. Rev. A **86**, 053401 (2012).
[20] H. Hattermann, M. Mack, F. Karlewski, F. Jessen, D. Cano, and J. Fortágh, Detrimental adsorbate fields in experiments with cold Rydberg gases near surfaces, Phys. Rev. A **86**, 022511 (2012).
[21] K. S. Chan, M. Siercke, C. Hufnagel, and R. Dumke, Adsorbate Electric Fields on a Cryogenic Atom Chip, Phys. Rev. Lett. **112**, 026101 (2014).
[22] A. Tauschinsky, R. M. T. Thijssen, S. Whitlock, H. B. van Linden van den Heuvell, and R. J. C. Spreeuw, Spatially resolved excitation of Rydberg atoms and surface effects on an atom chip, Phys. Rev. A **81**, 063411 (2010).
[23] R. P. Abel, C. Carr, U. Krohn, and C. S. Adams, Electrometry near a dielectric surface using Rydberg electromagnetically induced transparency, Phys. Rev. A **84**, 023408 (2011).
[24] T. F. Gallagher, *Rydberg Atoms*, 1st ed. (Cambridge University Press, Cambridge, England, 1994).
[25] J. M. McGuirk, D. M. Harber, J. M. Obrecht, and E. A. Cornell, Alkali-metal adsorbate polarization on conducting and insulating surfaces probed with Bose-Einstein condensates, Phys. Rev. A **69**, 062905 (2004).
[26] D. A. Hite, Y. Colombe, A. C. Wilson, K. R. Brown, U. Warring, R. Jördens, J. D. Jost, K. S. McKay, D. P. Pappas, D. Leibfried, and D. J. Wineland, 100-Fold Reduction of Electric-Field Noise in an Ion Trap Cleaned with In Situ Argon-Ion-Beam Bombardment, Phys. Rev. Lett. **109**, 103001 (2012).
[27] *The Physics of SiO2 and Its Interfaces*, edited by S. T. Pantelides (Pergamon, New York, 1978).

[28] S. S. Nekrashevich and V. A. Gritsenko, Electronic structure of silicon dioxide (a review), Phys. Solid State **56**, 207 (2014).

[29] S. Ismail-Beigi and S. G. Louie, Self-Trapped Excitons in Silicon Dioxide: Mechanism and Properties, Phys. Rev. Lett. **95**, 156401 (2005).

[30] P. F. Weck, E. Kim, and G. W. Biedermann, Interaction of cesium adatoms with free-standing graphene and graphene-veiled SiO2 surfaces, RSC Adv. **5**, 38623 (2015).

[31] R. H. Miwa, T. M. Schmidt, W. L. Scopel, and A. Fazzio, Doping of graphene adsorbed on the a-SiO2 surface, Appl. Phys. Lett. **99**, 163108 (2011).

[32] N. T. Cuong, M. Otani, and S. Okada, Semiconducting Electronic Property of Graphene Adsorbed on (0001) Surfaces of SiO2, Phys. Rev. Lett. **106**, 106801 (2011).

[33] J. Yang and E. G. Wang, Water adsorption on hydroxylated α-quartz (0001) surfaces: From monomer to flat bilayer, Phys. Rev. B **73**, 035406 (2006).

[34] N. H. de Leeuw, F. M. Higgins, and S. C. Parker, Modeling the surface structure and stability of α-quartz, J. Phys. Chem. B **103**, 1270 (1999).

[35] M. W. Cole, Electronic surface states of liquid helium, Rev. Mod. Phys. **46**, 451 (1974).

[36] C. Grimes, Electrons in surface states on liquid helium, Surf. Sci. **73**, 379 (1978).

[37] E. Andrei, *Two-dimensional Electron Systems: On Helium and Other Cryogenic Substrates* (Springer Science & Business Media, New York, 2012), Vol. 19.

[38] A. Safavi-Naini, P. Rabl, P. F. Weck, and H. R. Sadeghpour, Microscopic model of electric-field-noise heating in ion traps, Phys. Rev. A **84**, 023412 (2011).

[39] See Supplemental Material at http://link.aps.org/supplemental/10.1103/PhysRevLett.116.133201, for experimental details on the quartz surface preparation, MOT loading, Rydberg EIT, and photodesorption measurement and theoretical details of the density functional calculation and the model for the electrostatic adatom sticking on the surface, which includes Refs. [40–53].

[40] D. M. Harber, J. M. Obrecht, J. M. McGuirk, and E. A. Cornell, Measurement of the Casimir-Polder force through center-of-mass oscillations of a Bose-Einstein condensate, Phys. Rev. A **72**, 033610 (2005).

[41] J. P. Perdew, K. Burke, and M. Ernzerhof, Generalized Gradient Approximation Made Simple, Phys. Rev. Lett. **77**, 3865 (1996).

[42] P. E. Blöchl, Projector augmented-wave method, Phys. Rev. B **50**, 17953 (1994).

[43] G. Kresse and D. Joubert, From ultrasoft pseudopotentials to the projector augmented-wave method, Phys. Rev. B **59**, 1758 (1999).

[44] E. R. Davidson, in *Methods in Computational Molecular Physics*, NATO Advanced Study Institute, Series C Vol. 113, edited by G. H. F. Diercksen and S. Wilson (Plenum, New York, 1983), p. 95.

[45] M. Methfessel and A. T. Paxton, High-precision sampling for Brillouin-zone integration in metals, Phys. Rev. B **40**, 3616 (1989).

[46] H. J. Monkhorst and J. D. Pack, Special points for Brillouin-zone integrations, Phys. Rev. B **13**, 5188 (1976).

[47] J. Neugebauer and M. Scheffler, Adsorbate-substrate and adsorbate-adsorbate interactions of Na and K adlayers on Al (111), Phys. Rev. B **46**, 16067 (1992).

[48] R. F. W. Bader, *Atoms in Molecules: A Quantum Theory* (Oxford University Press, New York, 1990).

[49] W. Mönch, *Semiconductor Surfaces and Interfaces*, 3rd. ed. (Springer Science & Business Media, New York, 2013), Vol. 26.

[50] *CRC Handbook of Chemistry and Physics, 96th Edition*, edited by W. M. Haynes (CRC Press/Taylor and Francis, Boca Raton, FL, 2016).

[51] V. I. Polyakov, N. M. Rossukanyi, A. I. Rukovishnikov, S. M. Pimenov, A. V. Karabutov, and V. I. Konov, Effects of post-growth treatment and coating with ultrathin metal layers on the band bending and field electron emission of diamond films, J. Appl. Phys. **84**, 2882 (1998).

[52] K. P. Loh, J. S. Foord, R. G. Egdell, and R. B. Jackman, Effects of post-growth treatment and coating with ultrathin metal layers on the band bending and field electron emission of diamond films, Diamond Relat. Mater. **6**, 874 (1997).

[53] M. Eyckeler, W. Monch, T. Kampen, R. Dimitrov, O. Ambacher, and M. Stutzmann, Negative electron affinity of cesiated p-GaN(0001) surfaces, J. Vac. Sci. Technol. B **16**, 2224 (1998).

[54] J. de Boer, *The Dynamical Character of Adsorption*, 2nd ed. (Clarendon, Oxford, Clarendon, 1968).

[55] A. K. Mohapatra, T. R. Jackson, and C. S. Adams, Coherent Optical Detection of Highly Excited Rydberg States Using Electromagnetically Induced Transparency, Phys. Rev. Lett. **98**, 113003 (2007).

[56] J. M. Obrecht, R. J. Wild, and E. A. Cornell, Measuring electric fields from surface contaminants with neutral atoms, Phys. Rev. A **75**, 062903 (2007).

[57] M. Bouchiat, J. Guéna, P. Jacquier, M. Lintz, and A. Papoyan, Electrical conductivity of glass and sapphire cells exposed to dry cesium vapor, Appl. Phys. B **68**, 1109 (1999).

[58] M. Stephens, R. Rhodes, and C. Wieman, Study of wall coatings for vapor-cell laser traps, J. Appl. Phys. **76**, 3479 (1994).

[59] S. Gozzini, G. Nienhuis, E. Mariotti, G. Paffuti, C. Gabbanini, and L. Moi, Wall effects on light-induced drift, Opt. Commun. **88**, 341 (1992).

[60] I. I. Beterov, D. B. Tretyakov, I. I. Ryabtsev, A. Ekers, and N. N. Bezuglov, Ionization of sodium and rubidium nS, nP, and nD Rydberg atoms by blackbody radiation, Phys. Rev. A **75**, 052720 (2007).

[61] W. Li, M. W. Noel, M. P. Robinson, P. J. Tanner, T. F. Gallagher, D. Comparat, B. Laburthe Tolra, N. Vanhaecke, T. Vogt, N. Zahzam, P. Pillet, and D. A. Tate, Evolution dynamics of a dense frozen Rydberg gas to plasma, Phys. Rev. A **70**, 042713 (2004).

[62] J. D. Jackson, *Classical Electrodynamics*, 3rd ed. (Wiley, New York, 1999).

[63] S. D. Brorson, D. J. DiMaria, M. V. Fischetti, F. L. Pesavento, P. M. Solomon, and D. W. Dong, Direct measurement of the energy distribution of hot electrons in silicon dioxide, J. Appl. Phys. **58**, 1302 (1985).

[64] J. Ristein, *Thin-Film Diamond II*, Semiconductors and Semimetals Vol. 77, edited by C. E. Nebel and J. Ristein (Elsevier, New York, 2004).

[65] G. Kresse and J. Furthmüller, Efficient iterative schemes for ab initio total-energy calculations using a plane-wave basis set, Phys. Rev. B **54**, 11169 (1996).

[66] L. J. Brillson, *Surfaces and Interfaces of Electronic Materials* (John Wiley & Sons, New York, 2010), Vol. 7.

[67] P. Mori-Sánchez, A. J. Cohen, and W. Yang, Localization and Delocalization Errors in Density Functional Theory and Implications for Band-Gap Prediction, Phys. Rev. Lett. **100**, 146401 (2008).

[68] A. J. Cohen, P. Mori-Sánchez, and W. Yang, Challenges for density functional theory, Chem. Rev. **112**, 289 (2012).